AFRL-RV-PS-
TR-2016-0162

PHYSICS OF COUPLED CME AND FLARE SYSTEMS

K. S. Balasubramaniam, et al.

21 December 2016

Final Report

AIR FORCE RESEARCH LABORATORY
Space Vehicles Directorate
3550 Aberdeen Ave SE
AIR FORCE MATERIEL COMMAND
KIRTLAND AIR FORCE BASE, NM 87117-5776

DTIC COPY

NOTICE AND SIGNATURE PAGE

AFRL-RV-PS-TR-2016-0162 HAS BEEN REVIEWED AND IS APPROVED FOR PUBLICATION IN ACCORDANCE WITH ASSIGNED DISTRIBUTION STATEMENT.

//SIGNED//	//SIGNED//
Dr. Karatholuvu S. Balasubramaniam	Dr. Thomas R. Caudill, Acting Chief
Program Manager, AFRL/RVBXT	AFRL Battlespace Environment Division

REPORT DOCUMENTATION PAGE

Form Approved
OMB No. 0704-0188

1. REPORT DATE *(DD-MM-YYYY)*	**2. REPORT TYPE**	**3. DATES COVERED** *(From - To)*
21-12-2016	Final Report	01 Apr 2014 to 30 Sep 2016

4. TITLE AND SUBTITLE
Physics of Coupled CME and Flare Systems

5a. CONTRACT NUMBER

5b. GRANT NUMBER

5c. PROGRAM ELEMENT NUMBER
61102F

6. AUTHOR(S)
K. S. Balasubramaniam, R. Hock-Mysliwiec, M. Kirk, L. Winter, and T. Henry

5d. PROJECT NUMBER
3001

5e. TASK NUMBER
PPM00016108

5f. WORK UNIT NUMBER
EF122003

7. PERFORMING ORGANIZATION NAME(S) AND ADDRESS(ES)
Air Force Research Laboratory
Space Vehicles Directorate
3550 Aberdeen Avenue SE
Kirtland AFB, NM 87117-5776

8. PERFORMING ORGANIZATION REPORT NUMBER
AFRL-RV-PS-TR-2016-0162

9. SPONSORING / MONITORING AGENCY NAME(S) AND ADDRESS(ES)

10. SPONSOR/MONITOR'S ACRONYM(S)
AFRL/RVBXT

11. SPONSOR/MONITOR'S REPORT NUMBER(S)

12. DISTRIBUTION / AVAILABILITY STATEMENT

Approved for public release; distribution is unlimited. (OPS-17-12901 dtd 02 Feb 2017)

13. SUPPLEMENTARY NOTES

14. ABSTRACT

Geo-effective solar eruptions can be traced to coupled coronal mass ejection (CME) and flare in solar active regions. This proposal is aimed at understanding conditions in the solar atmosphere leading to solar eruptions that are geo-effective, and to develop models to understand these coupled eruptions. The component objectives for this task were: (i) derive measureable physical properties and discernible structural circumstances in solar active regions that produce near-simultaneous large flares and coronal mass ejections (CMEs), when compared to those regions or circumstances in those regions that produce only flares or CMEs, in isolation, and (ii) develop statistical models for identifying those signatures and physical attributes that possibly lead to eruption of combined flare-CME systems, as opposed to flares or CME in isolation. This work uses solar synoptic imaging and irradiance data from both ground and space-based observatories. The technical approach to this work was built on research done at AFRL and includes methods of image processing, numerical analysis, and model fitting such as active region identification, feature tracking, statistical analysis (including regression analysis, principal components, machine learning and discriminant analysis), classification algorithms, and magnetic field modeling.

15. SUBJECT TERMS
Solar Flares, Coronal Mass Ejections, CMEs, Space Weather Effects

16. SECURITY CLASSIFICATION OF:			**17. LIMITATION OF ABSTRACT**	**18. NUMBER OF PAGES**	**19a. NAME OF RESPONSIBLE PERSON**
a. REPORT	**b. ABSTRACT**	**c. THIS PAGE**			Dr. Karatholuvu S. Balasubramaniam
Unclassified	Unclassified	Unclassified	Unlimited	30	**19b. TELEPHONE NUMBER** *(include area code)*

This page is intentionally left blank.

Table of Contents

List of Figures

Acknowledgments

This work was supported and funded by the Air Force Office of Scientific Research (AFOSR). We express gratitude to Drs. Kent Miller and Julie Moses, AFOSR for enabling this work. Our gratitude to the leadership and critical personnel at the Space Vehicles Directorate, AFRL & its Space Environment Branch who enabled the execution of the work, during its various phases. This report provides the final summary of the work performed under this AFOSR task, supported by individual and interim technical work which has been published in peer-reviewed journals and presented in professional society meetings as appropriate. This final report and relevant research was supported by technical collaborators: R. Hock-Mysliwiec, M. Kirk, L. Winter, and T. Henry. We express gratitude to the National Solar Observatory, Air Force Research Laboratories, NASA Goddard Space Flight Center, Lockheed Martin Solar and Astrophysics Research, Stanford University, U. Colorado at Boulder, NASA's Solar Dynamics Observatory, NOAA's Space Weather Forecast Center, and numerous individuals from these organizations who helped us with using data, models and understanding their state-of-art applications. Data sources for the work described elsewhere in individual research papers include the National Solar Observatory, NOAA Space Environment Center, NASA/SOlar and Heliophysics Observatory (SOHO), NASA/Solar Dynamics Observatory (SOHO), and AFRL's ISOON Prototype telescope are acknowledged in the appropriate individual publications. The Interactive Data Language (IDL) was used for much of the analysis in this study.

This page is intentionally left blank.

1. SUMMARY

The constituent component of solar eruptions, including solar flares, coronal mass ejections (CMEs) and filament eruptions, constitute the major solar sources of space weather. Solar eruptions have been traced back to solar active regions. The interactions of the solar magnetic fields with the plasma are complex. The plasma properties of the surface solar active region plasma are modulated along its magnetic fields by changes in thermodynamic conditions in the various layers of the solar plasma (photosphere, chromosphere & corona), as its magnetic fields are themselves modulated by the underlying solar cycle. The eruptions are manifested due to the release of built-up energies in the various layers, driven by both global and local magnetohydrodynamic instabilities. Solar active regions represent physical systems with underlying properties that can be characterized, explained and threaded into physical and statistical models. These models can then be used to heuristically develop tools for tracking potentially eruptive systems, and to predict and forecast impending eruptive activity. Such information can be used by DOD operators to mitigate the potentially known impacts to space assets and ground systems involving communication, navigation, position, and timing needs. This also supports a need to distinguish space weather impacts to system from human interference.

The work presented here summarizes a three-year effort to understand and characterize aspects of the physics of coupled flare and CME systems. Parallel tracts were undertaken to understand individual signatures of flare and CME systems, as well as understanding their aggregate behavior during the solar cycle. The component of this work include the understanding the (i) physics properties of Sequential Chromospheric Brightenings (SCBs) that occur as precursor signatures of coupled flare-CME systems, both individually and in aggregate, (ii) statistically understanding solar flares and CMEs in an effort to characterize their solar cycle behavior and their predictability, (iii) and to characterize the solar spectral irradiance in solar loops; as heating in solar loops from solar flares, in turn drive the radiative heating of ionosphere.

2. INTRODUCTION

Solar flares are the localized (a few arcseconds across, e.g**.** Shibata & Magara 2011 **[1]**), catastrophic release of energy in the solar atmosphere, which lasts minutes to hours and results in the heating of plasma, mass ejection, and particle acceleration. Solar flares also cause an increase in radiation across the entire electromagnetic (EM) spectrum. As different parts of the spectrum originate in the different layers of the solar atmosphere (photosphere, chromosphere, and corona), the changes across the EM spectrum are non-uniform and reveal information about the fundamental processes that occur during a flare.

Solar flares can be separated into confined and eruptive flares (e.g. Svestka & Cliver 1992 **[2]**). While a confined flare does not change the overlying magnetic structure in the flaring region (Aschwanden et al. 2009, **[3]**), an eruptive flare results in mass leaving the flaring region as seen in images of the solar corona and is often associated with a coronal mass ejection (CME) as observed by a white-light coronagraph.

CMEs are spectacular, large-scale solar eruptions extending outward from the corona spanning several arcminutes and are associated with solar flares. A typical CME carries between 1×10^{12} and 5×10^{13} kg of material, about one-tenth of the total mass of the corona, at speeds between 100 and 3400 km s^{-1} (Lang 2009 **[4]**). The earliest (temporal) indicators of CMEs appear in images of the solar atmosphere as sequential chromospheric brightenings (SCBs; Balasubramaniam et. al. 2005**[5]**), chromospheric (Moreton) and coronal (EUV) waves (Balasubramaniam et al. 2007 **[6]**, Thompson et al. 1999 **[7]**), and coronal dimmings or decreases in the brightness of large regions of the solar atmosphere (e.g. Reinard & Biesecker 2008**[8]**). Following the surface detection, white-light coronagraphs and heliospheric imagers observe a CME as it propagates through the heliosphere (Gopalswamy et al. 2009 **[9]**). CMEs are important for understanding the driver of solar energetic particles (SEPs); SEPs are a major source of single-event upsets of spacecraft and are accelerated by CME-driven shock waves (Reames, 2000) **[10]**.

The objectives of this work were to understand the physics of coupled CME and flare systems from (i) individual intensity and magnetic field measurements of active regions to understand the spatial, structural and thermal components of active regions; (ii) collective flaring statistics of sunspot numbers, flares and CMEs in order to characterize their solar cycle behavior; and (iii) the heating of flares loops and their model reproduction, in an effort to reproduce the aggregate behavior of flare emissions.

In order to diagnose the physical conditions in solar active regions that lead to eruptive events, we examined images of eruptive events using a number of observable layers that span from the low photosphere and into the corona. We used techniques to include methods of image processing, numerical analysis, and model fitting such as active region identification, feature tracking, statistical analysis (classification algorithms, and magnetic field modeling.
The physical properties we explored include: intensities of photospheric, chromospheric and coronal bands; sunspot areas, plage area and intensities in the chromosphere; changes in the magnetic field quantities (flux, area, spatial gradients); spatial variation of features and their relationships to emission and modeled structural components of the magnetic fields. Using the non-linear force free models, analyzed spatial locations for flare heating, chromospheric brightenings, loop positions. We took consideration that aspects of the same active region during different phases of its life-time might produce eruptive events. In addition, we will use the publically available CME catalogs and flare event lists as well as irradiance spectra from SDO/EVE to develop a models of heating and apply it to the active regions. We sorted to sort the events based on this metric and sought commonalities in the active region characteristics to understand the nature of the events as a function of the solar cycle.

Below we describe each sub-effort and summarize the results.

3. METHODS, ASSUMPTIONS, PROCEDURES, AND RESULTS

3.1 Understand Sequential Chromospheric Brightenings (SCBs) at edge of flare-CME systems.

Basis: Sequential Chromospheric Brightenings (SCBs) occur at periphery of flare-CME sites.

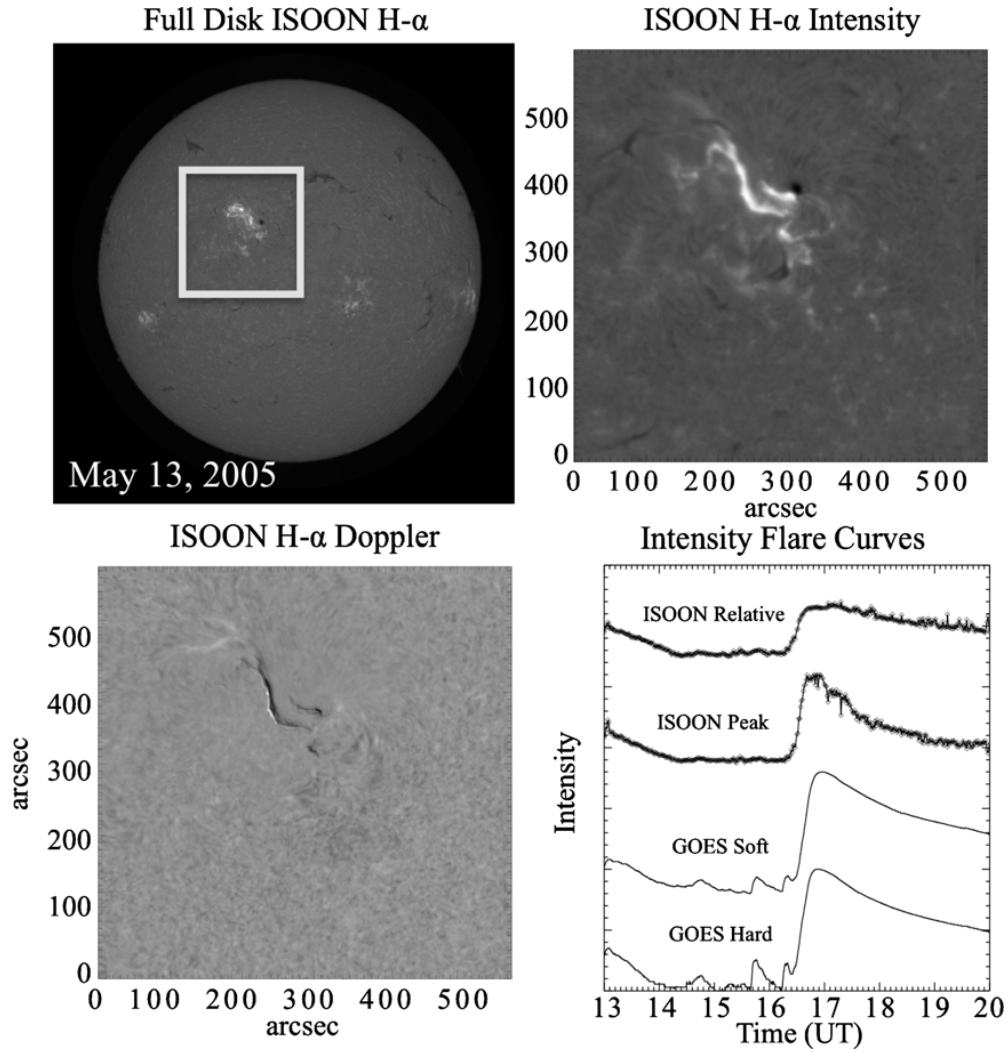

Figure 1: A Solar flare captured in solar chromospheric Ha, using the ISOON telescope, as a representative sample, obtained 2005 May 13. *The bright ribbons are the flare brightenings. The flare evolution is captures on a series of 1-minute cadence, 1.1 arcsecond sampled images.*

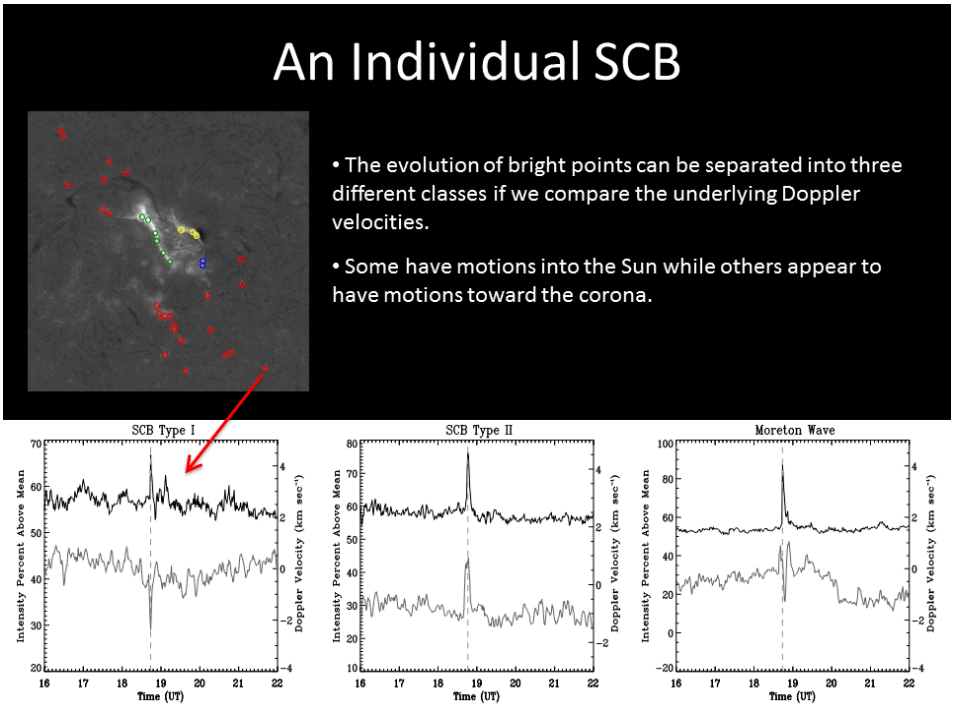

Figure 2: The individual SCBs are marked as circles. *The bottom panels describe 3 types of SCBs obtained with ISOON data.*

They occur as a spatial train of brightenings – minutes to seconds before flaring (see Figure 1). [**5**].They are accompanied by filament eruption. They originate during impulsive rise-phase, precede Hα flare intensity SCBs are attributed to compact chromospheric ablation by electron precipitation – **[11-12].**

We used the Improved Solar Observing Optical Network (ISOON, **[13]**) prototype telescope (Doppler, Ha) and Solar Dynamics Observatory (1700 A, 1600 A, 304 A; **[14]**) imagery data to track and characterize SCB median diameter, median duration and ensemble motion. Two-ribbon flaring event from 2005 May 13 (Figure 1) shows an example of a calibrated Hα ISOON image with the region of interest (RIO), highlighted. The ISOON image are 2048 × 2048 pixels with each pixel having a 1.1" resolution. The bottom panel in Figure 1 (below) is the ROI after preprocessing. This ROI covers 576 × 576 pixels corresponding to 2.12 × 1011 km^2 on the solar surface. Figure 2 is a Doppler measure of the same ROI. The Doppler velocity image is created out of ISOON Hα off-band images where the velocity ranges from −26.6 to 21.5 km s−1 from black to white (see Figure 1). Panel (d, Figure 1) shows intensity curves over the time period of interest: 13:00–20:02 UT and trace a flare curve.

Table 1 traces the median size and duration of SCBs. Here one notices that flares last longer than SCBs, while their structure is compact.

Table 1: Size & duration of SCBs

Kernel Type	Median Diameter	Median Duration	Ensemble Motion
Flare	6.4 Mm	64 mins	Directional
SCB	2.4 Mm	9.9 mins	Random Walk

We calculated the radiating cooling and heating time of SCBs. The radiative cooling time is given by

$$t_{\rm rad} \simeq \frac{3kT}{nQ(T)} \simeq 5 \times 10^3 \text{ s} \left(\frac{T}{10^6 \text{ K}}\right)^{3/2} \left(\frac{n}{10^9 \text{ cm}^{-3}}\right)^{-1},$$

While the radiative heating time of the SCB is calculated to be $t_{heating}$ = 2.8 s.

$$10^{27} \text{ erg} \leqslant \sum_{\text{event}} E_{\rm SCB} \leqslant 10^{28} \text{ erg},$$

This results in the energy budget bounds of a single SCB . Hence, for all SCB's in a flare, the total enegy is:

$\sum E_{\rm SCB} \geqslant 10^{31}$ ergs

k is Boltzmann's constant,
Q(T) is the radiative loss function for optically thin plasma at
temperature, T
n is the number density of atoms.

This is about 10% of the flare energy. Resultantly, there are

- Three distinguishable types of SCBs, which is consistent with Kirk et al. 2012 **[15], [16]**.
- Shorter duration in corona (4 minutes) when compared with chromosphere (~10 minutes)
- Peak intensity at Corona delayed by ~ 1 minute after chromosphere
- SCBs are formed in the mid-chromosphere and propagate vertically upward toward the transition region and downward toward the photosphere.

The application of these results helps is that SCBs when tracked can aid in detection of flare peaks by about 4 minutes in advance for large flares

SCBs occur at periphery of flare-CME sites. They ae precursors to large solar flares coupled with CMES as a part of the M and X class flare systems. We used the automated detection algorithm of Kirk et al. [16] to extract the physical qualities of SCBs in 14 fares of varying size and intensity. The events used in this work to investigate the automated identification and tracking of SCBs and flare ribbons. The time listed is the start time of the flare or filament eruption. Twelve of the fourteen events were previously identified by Balasubramaniam et al. (2005; **[5]**),

Balasubramaniam et al. (2006 **[17]**), Kirk et al. (2012a; **[15]**), Kirk et al. (2012b **[16]**), or Kirk et al. (2014; [**18]**) labeled Ba, Bb, Ka, Kb or Kc respectively, while two are new in this study. The data sources utilized for each event are abbreviated as: ISOON, LASCO, GOES, MDI, and CACTus. We conclude that SCBs originate in the lower corona around 0:1 R. above the photosphere, propagate away from the flare center at speeds 35 - 85 km kms/s and have typical photosphere magnetic intensities < 50 Gs. In light of these measurements, we infer SCBs to be distinctive chromospheric signatures of erupting coronal mass ejections.

Table 2: The events used in this work to investigate the automated identification and tracking of SCBs and flare ribbons. The time listed is the start time of the flare or filament eruption.

Date	Time UT	GOES Class	Visual CME	Data Sources	Previously Studied
2002-12-13	21:35	C6.8	yes	I, L, G, C	Ba
2002-12-19	21:34	M2.7	yes	I, L, G, M, C	Bb & Kb
2003-01-24	22:04	C1.3	no	I, L, G	Ba
2003-02-06	16:30	None	yes	I, L, G, C	Ba
2003-03-06	15:08	None	no	I, L, G, M	no
2003-05-09	15:18	B6.6	yes	I, L, G, M, C	Bb
2003-06-11	17:27	M1.8	no	I, L, G, M	Bb
2003-10-29	20:37	X10.0	yes	I, L, G, M, C	Bb
2004-11-09	16:59	M8.9	yes	I, L, G, M, C	Bb & Ka
2005-05-06	16:03	C8.5	yes	I, L, G, M, C	Bb & Ka
2005-05-13	16:13	M8.0	yes	I, L, G, M, C	Ka
2006-12-06	18:29	X6.5	yes	I, L, G, M, C	Kb
2010-11-06	15:30	M5.4	yes	I, L, G, M, C	Kc
2010-11-30	17:35	None	yes	I, L, G, M, C	no

We conclude that SCBs originate in the lower corona around 0:1 R. above the photosphere, propagate away from the flare center at speeds 35 - 85 km/s and have typical photosphere magnetic intensities < 50 Gs. In light of these measurements, we infer SCBs to be distinctive chromospheric signatures of erupting coronal mass ejections.

Magnetic Model for SCBs

Using the SDOs' [**14**] Heliospheric Magnetic Imager's magnetic field measures, we modeled the magnetic file of solar active regions, particularly in an effort to understanding the magnetic structure of SCBs. We used the Potential Field Source Surface (PFSS) models to understand evolutionary characteristics of the SCB eruptions[**19**]. The resulting model calculations shows the progress of such an eruption in Figure 3.

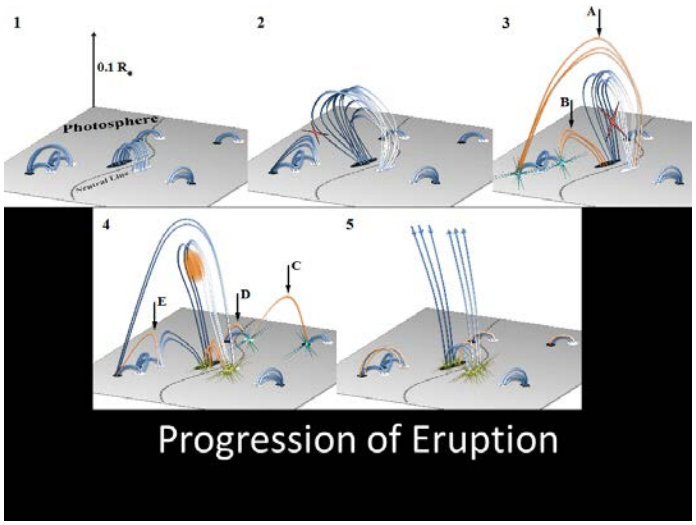

Figure 3: PFSS modeling of SCBS. *Progression of a solar flare and resulting loops shown at marked positions of overarching field lines A, B, C, D and E.*

Figure 3 shows flux rope eruption moving beyond the local region depicted and the dipolar and quadrupolar regions relaxing into a potential field configuration. Notice that one dipolar region remained unchanged throughout the eruption. This is due to the physical geometry of the eruption itself. Two ribbon flares have an elongated axis that makes it favorable for field lines to connect to regions tangentially aligned with this axis. Regions that are perpendicular to this flare axis are more resilient to reconnection with the flare arcade and thus less prone to SCBs. (See: **[20]**.

Our summary findings on SCBs are: SCBs originate in quiescent coronal magnetic loops. Almost all (79%) SCB events are followed by complementary CMEs. SCBs propagate away at two distinct speeds: between 35 and 85 km/s and >150 km/s. Flare intensity class does not impact propagation speeds or likelihood of detection. SCBs have monopolar foot points with intensities <50 G. The origin of SCBs is in the lower corona at heights around 0.1 Rsun above the surface.

3.2 Collective flaring statistics of sunspot numbers, flares and CMEs in order to characterize their solar cycle behavior

Understanding solar cycle behavior is important to characterizing solar flare activity. Among the fist are sunspot numbers.
Sunspot Numbers are important tracers of historical solar activity. They are important in the prediction of oncoming solar maximum, in the design of life-times of space assets, and the extent of solar radiation impact on space environment. Sunspot numbers were obtained visually from sunspot drawings. The availability of digital images from the US Air Force Improved Solar Optical Observing Network (ISOON) prototype telescope concurrent to observer dependent sunspot numbers recorded at Sacramento Peak Observatory and the National Solar Observatory (NSO) has provided a basis for comparing sunspot numbers determined from the two methods.

Using the ISOON digital sunspot numbers demonstrated the advantages of using consistent digital sunspot images and the insights gained from analyzed sunspot numbers from both sunspot drawings and digital data. We have established a coherent comparison mechanism of counting Sunspot numbers from both sources, and trace potential errors when comparing older sunspot numbers to recent digital data. We have also shown the advantage of intra-day variation of sunspot areas as an alternate to sunspot numbers where digital data is available; however, we have established the conversion metrics to go between sunspot numbers and sunspot areas measures, as needed to the context of the research.

The merging of digitized continuum images with projection board drawings as a means to compute Wolf numbers provides a better picture of solar activity. One can characterize what was seen on the projection board. To understand and develop an effective conversion between the two methods under similar conditions, digital images need to be acquired about nearly the same time as projection board drawings, at similar, if not identical, locations. This paper demonstrates such an effort. A projection board drawing requires an observer to be sitting at the telescope actively drawing and counting sunspots. If one is unavailable the opportunity is lost. Any drawing made is not reviewable, though it may be compared with other observations by other observers elsewhere and at different times. In contrast, a digital image can be reassessed as its analysis can be adjudicated at any time in the future.

Sunspots can emerge or dissipate at any point in an observing period. Often faint spots can be seen in an image, persist from image to image and yet be below threshold. Fading in and out they may or may not be seen on a projected image. The question arises on whether to ignore these spots or count them in some way. A researcher needs to be cognizant that counting sunspots may drastically increase the R number, and use the results appropriate to the context. One such example was on 2003 October 13, when the south-west part of the Sun, close to the disk center showed visual persistent spots. However, the corresponding digital counts showed no such spots, because they were below the intensity threshold.

In general, imagery from ISOON detects many more spots and groups than ISN suggest, but there are many exceptions. Some of the difference will be in the method of counting spots, or identification of penumbra versus umbra. However, counting umbrae will greatly exaggerate this difference which can be alleviated by determining minimum threshold such as in area or darkness to define a sunspot.

Comparison was also made between ISOON spot counts and NOAA/Space Weather Prediction center counts that are immediately available before reconciliation. SWPC uses the USAF's operational SOON telescope network's projection board drawings in processing the data. Despite better seeing conditions for ISOON (at high altitude where Sac Peak is located), preliminary spot counts reported by NOAA-USAF were consistently greater and often double those seen with ISOON imagery. For example, from 2008 January 01 to 2011 March 31 there were 609 common observations for ISOON and NOAA reports. More than ten percent of the time reports registered more than double ISOON spot counts.

An image is a means to verify the existence of an active region from an observatory. The method used to assign NOAA active region numbers can have the effect that active regions may be several days old before being identified. In addition, one must be aware the NOAA active region number assignment can be temporally stale by as much as a whole day. In our experience at NSO, numerous one and two day events, where new active regions are not numbered, were

noted. A one day event may be understood as observations at NSO in New Mexico are relatively late in the observing day as compared to other observatories around the world. As confirmation of a region requires observations twelve hours apart, a two day event may be understood as observatory downtime and a region observed by the same observatory over two days before confirmation.

In tracking the intra-day variation of solar activity, we have demonstrated that sunspot component measures, such as umbral and penumbral areas and intensities, dramatically change during and after large solar flares. The underlying changes in sunspot areas cannot be reflected in sunspot numbers, which are coarser measures of solar activity on time-scales of a day or more. Integrated sunspot areas and irradiance deficits can be diagnostics of alternate measures of solar activity to monitor finer changes. The important point here is that sunspot imagery and quantitative changes are better reflected in measures of component solar activity than those represented by sunspot number changes, when considering finer representations of solar activity in the context.

If one were to construct a network of telescopes, as was planned for ISOON, issues to be resolved would include standardization of wavelength, filter width and aperture of a candidate telescope. A high resolution telescope will see very fine spots and can be expected to see more than the human eye. Integrated over time, a more accurate picture of solar activity can be obtained from a telescope with multiple images than a single observation once a day. These results were summarized in **[21].**

Comparing Sunspot Number Index to X-ray Flare and Coronal Mass Ejection rates.

Understanding the x-ray flare variations with sunspot was the next research target. We used the GOES soft and hard x-ray data to analyze the background subtracted solar flare emission, and developed a machine level algorithm to characterize the strength of flares based on the background radiation. Here we understood that the solar background acts as a thermal elevator that is ready to flare depending on the background strength. We discovered a relationship between the maximum ratio of the flare flux (namely, 0.5–4 Å to the 1–8 Å flux) and non-flare background (namely, the 1–8 Å background flux), which clearly separates flares into classes by peak flux level. We established this relationship based on an analysis of the Geostationary Operational Environmental Satellites X-ray observations of ~ 50,000 X, M, C, and flares derived from the NOAA/Space Weather Prediction Center flares catalog. Employing a combination of machine learning techniques (K-nearest neighbors and nearest centroid algorithms) we show a separation of the observed parameters for the different peak flaring energies. This analysis is validated by successfully predicting the flare classes for 100% of the X-class flares, 76% of the M-class flares, 80% of the C-class flares, and 81% of the B-class flares for solar cycle 24, based on the training of the parametric extracts for solar flares in cycles 22–23. This flare phase diagram, is shown in figure 4.

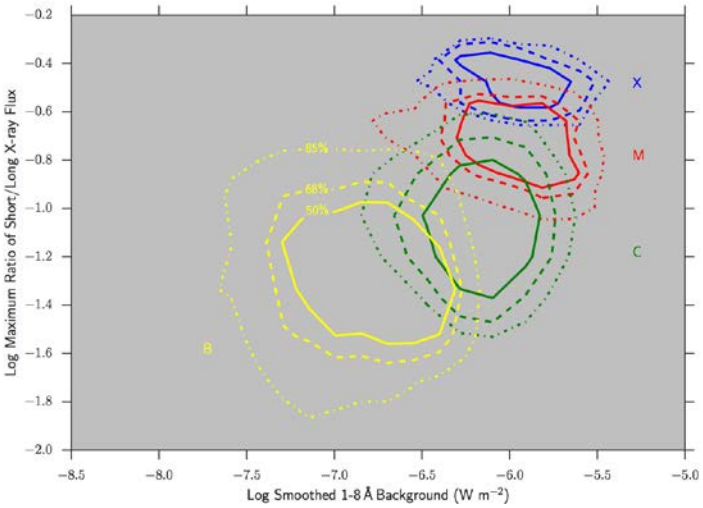

Figure 4: A phase diagram for solar flares. *The ratio of the solar short to long wavelength x-ray varies as a function of the strength of the solar background.*

The real-time background (B) and ratio (R) are input into statistical models to predict flare class The predictions are made based on previous analysis of the B and R parameters from 50,000 flares from 1986-2015 Two prediction models are used with machine-learning algorithms of Nearest Centroid and K-Nearest Neighbor.

Using the two models we developed a prototype flare forecast system shown in Figure 5. These results were published in **[22]**

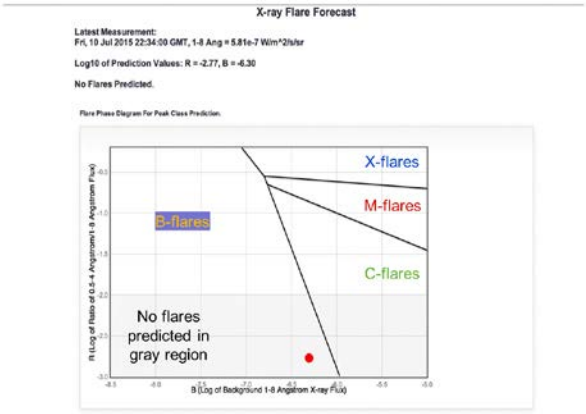

Figure 5: A real-time prototype forecast system using the x-ray background radiation and the ratio of the soft-to-hard x-ray peak flux, using a flare phase diagram. *The various flare categories are shown. The red dot indicates a flare probability location for July 10 2015 at 22:34 UT.*

In a related study, we examined the sunspot number relationship to the coronal mass ejection rates for solar cycles 23-24. The newly revised sunspot number series allows for placing historical geoeffective storms in the context of several hundred years of solar activity. Using statistical analyses of the GOES X-ray observations from the past 30 years and the SOHO/LASCO CME catalog (1996-present), we present sunspot number dependent flare and CME rates. In particular, we present X-ray flare rates as a function of sunspot number for the past three cycles.

We also show that the 1-8 A X-ray background flux is strongly correlated with sunspot number across solar cycles. Similarly, we show that the CME properties (e.g., velocity and width) are also correlated with sunspot number for cycles 23 and 24. These updated rates will enable future predictions for geoeffective events and place historical storms in context of present solar activity. [**23**]

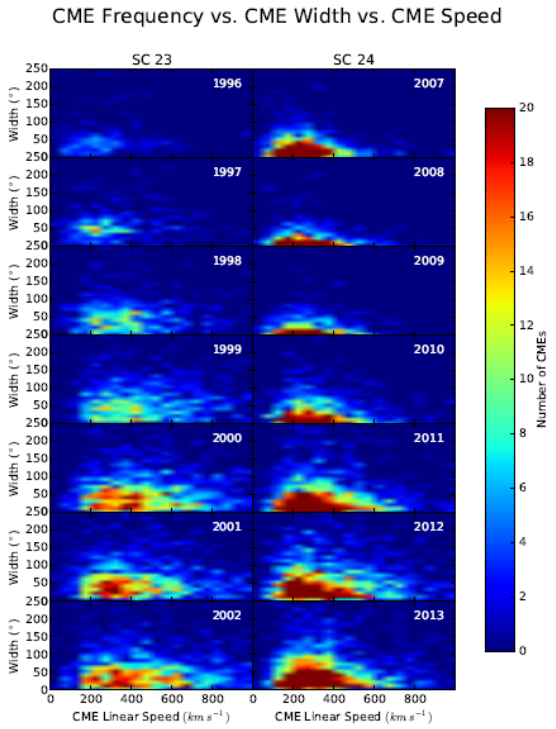

Figure 6: 2D histograms of CME frequency as a function of angular width and speed. *The first column is approximately the first 7 years of SC (Solar Cycle) 23; the second column is the corresponding 7 years of SC24. Each row represents 2 distributions from identical phases in different solar cycles. For example, 1996 and 2007 are in the same row and are solar minimum years for SC23 and SC24, respectively. The histograms are presented on the same color scale so that the disparity in CME frequency for identical phases is apparent. Solar cycle dependence of CME frequency and speed is also clear when examining a single column {the histogram structures widen along the speed axis and become more intense (redder) as one proceeds from solar minimum to solar maximum. There are far more CMEs recorded in SC24 with widths <50°, as well.*

3.3 The AF Irradiance Model - Characterize the solar spectral irradiance in solar loops.

A solar eruptive event (SEE) results from the sudden release of stored magnetic energy in the solar atmosphere. There are many manifestations of this energy release including solar flares, which are observed as:

- Soft X-ray (SXR) and Extreme Ultraviolet (EUV) flare loops and loop arcades
- Bright "ribbons" in the chromosphere at the footpoints of the flare loops
- Multiple hard X-ray sources, both at the footpoints and the apex of the flare loops
- Radio bursts

There are also non-flare manifestations such as coronal mass ejections (CMEs), Moreton and EUV waves in the chromosphere and corona respectively, and solar energetic particles.

While flares are usually classified by their peak brightness in the soft X-ray as measured by the NOAA GOES XRS instrument, the amount of the energy in the extreme ultraviolet determines the impact on the Ionosphere-Thermosphere. Using the correlation in Le et al. 2012 **[24]**, 18% of M-class and 35% of X-class flares are strong enough in the EUV to cause a >10% enhancement in the thermosphere density. At the same time, M-class flares can cause a spread in Doppler frequency at 10 MHz corresponding to 162 kph, large enough to impact Over the Horizon (OTH) systems (Hemlboldt et al. 2015; **[25]**).

The solar flare EUV spectral irradiance is a critical driver for future generations in Ionosphere-thermosphere models. Measuring EUV irradiance with sufficient spectral resolution and time cadence to capture the evolution of solar flares is hard. While there have been various sub-orbital rocket experiments since the late 1940s and early satellite programs such as Orbiting Solar Observatory (OSO) (1960s) and AE (1970s), the first routine measurements were made by NASA's TIMED/SEE. SEE has low spectral resolution and ~90 minute cadence, allowing it to make irregular observations of fortuitous flares. New (and better) observations are available from NASA's SDO/EVE. EVE has moderate spectral resolution and 10-second time cadence, making it ideal for studying the variability due to solar flares.

Modeling of flare spectral irradiance has its own challenges, in particular how to capture the observed temporal and spectral variability. At present, there is one flare irradiance model: the Flare Irradiance Spectral Model (FISM) developed at the University of Colorado and NASA. It is an empirical model based on TIMED/SEE observations and driven by GOES XRS. Figure 7 shows a comparison of FISM and observations from SDO/EVE for two EUV wavelengths for an X-class flare. Notice that FISM (blue) fails to capture the timing of the peak as well as missing the energy in the EUV late phase (the secondary emission after the main peak).

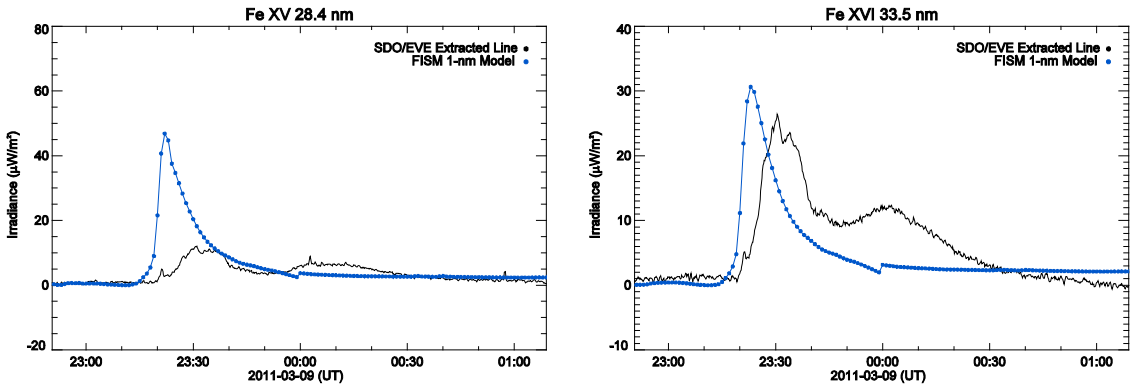

Figure 7: Comparisons of the FISM model with the EUV flare spectrum for an X-class flare.

Description of Model

The Air Force Flare Irradiance Model (AFFIM) using our physical understanding of how EUV flare emission forms to accurately capture the full range of variability observed by SDO/EVE. The EUV spectrum of the Sun is dominated by bound-bound emission lines. The strength or brightness of a line is related to the density of the plasma while each line is associated with a temperature. After the energy release during a flare, very hot (10s MK) plasma fills newly formed coronal loops. This hot plasma cools, emitting EUV photons. As the plasma temperature decreases, successively cooler emissions get stronger.

AFFIM is a numerical model, which as its core uses the EBTEL hydrodynamic code from NRL/NASA **[26-29]** to heat numerous flare loops, track the evolution of temperature, density, and pressure of each loop as they cool. From the output of the EBTEL code, the EUV spectrum over the course of the flare is calculated using the CHIANTI atomic database (www.chiantidatabase.org).

The model has several parameters. The first is the number of model loops, which is determined by the duration of the flare. Each loop has three parameters that are allowed to vary to optimize the model: peak heating rate, loop length, and loop cross-section. The inputs of AFFIM are light-curves of two EVE lines which are indicative of the behavior of hot and warm corona. The model uses non-linear least squares fitting to adjust the model parameters to closely reproduce the input EVE light-curves. Figure 8 shows the EVE input light-curves with the fitting window highlighted.

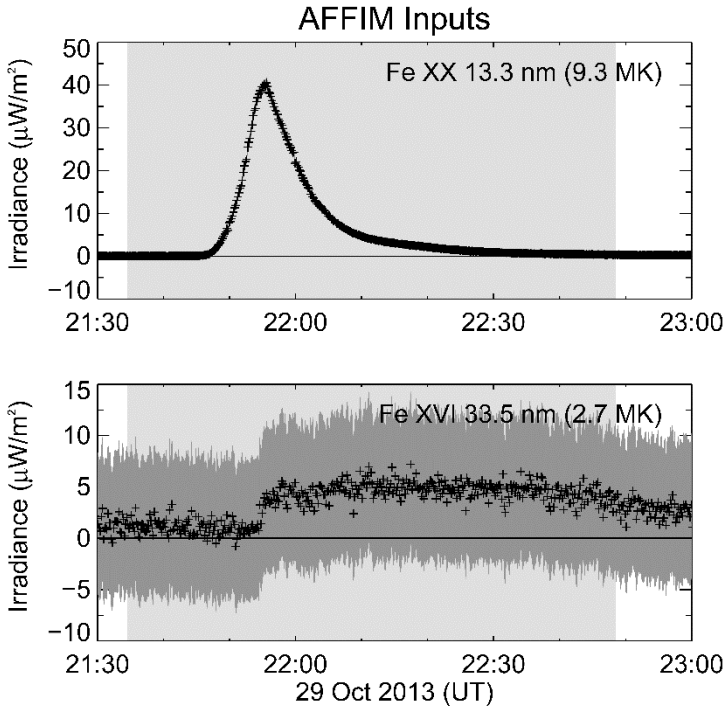

Figure 8: AFFIM Model Inputs - Light curves of individual spectra lines.

Figure 9 shows the best fit model parameters. The outputs of AFFIM are either light-curves of individual lines or model parameters Figure 9, or the spectrum as a function of time as in Figure 10.

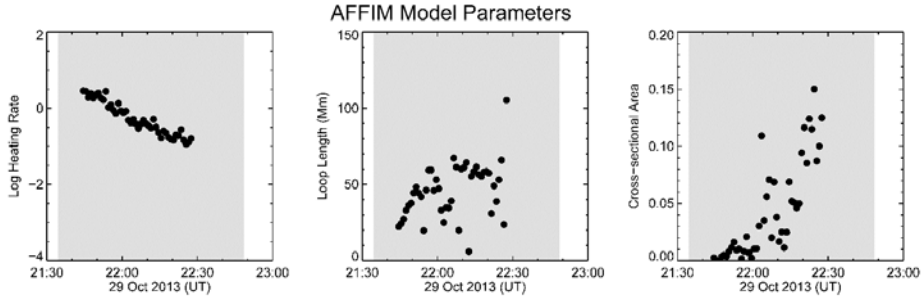

Figure 9: Light curves of individual spectral lines vary, depending on the AFFIM model.

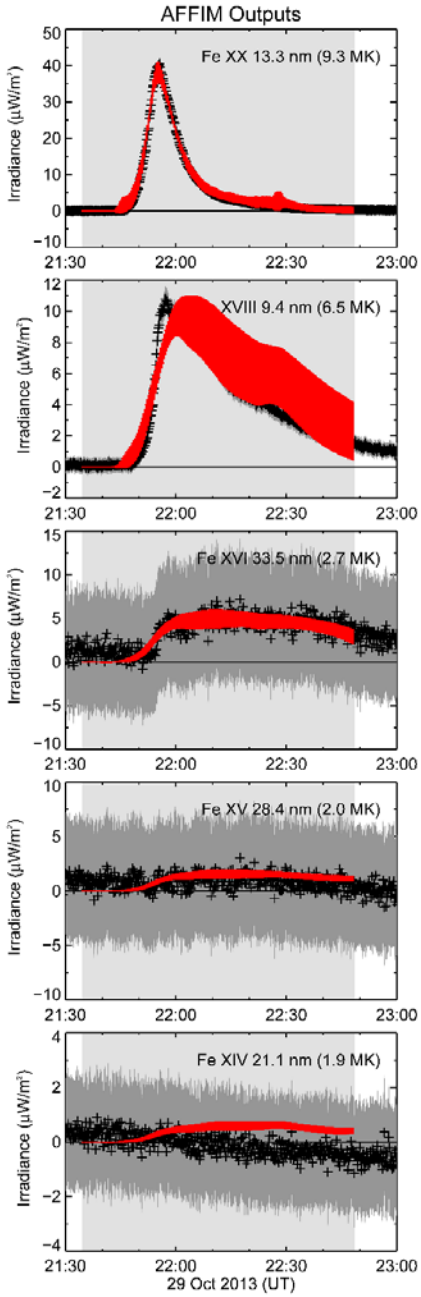

Figure 10: Temporal spectral outputs from the AFFIM model for different spectral lines.

Sensitivity Studies

AFFIM has been run semi-autonomously for >100 flares from 2010-2014. For each flare, 65 individual runs were done to capture the sensitivity to initial parameters and can used to determine the uncertainties in the individual light curves. Comparing the AFFIM output to EVE lines can be used to validate the model (Figure 11). Two lines are used as input and the model should reproduce those the best.

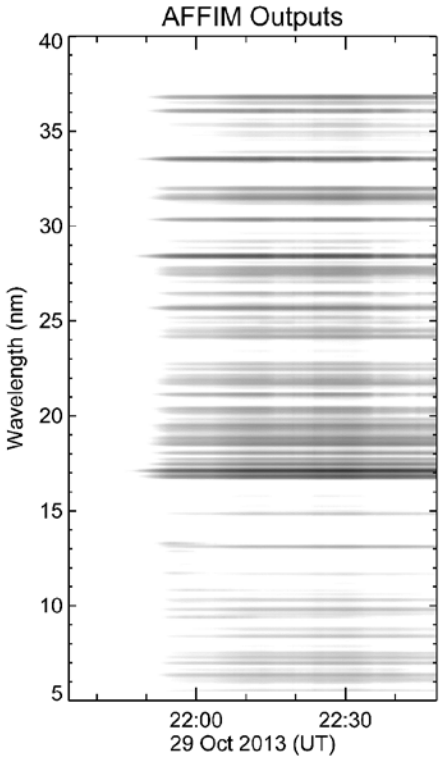

Figure 11: Spectral outputs of the AFFIM model.

Driving AFFIM with Images

The NASA/SDO EVE telescope stopped observing the Sun in 2014 so AFFIM cannot be run for recent or future solar flares. It would be advantageous if we could calculate the model parameters directly and independently. EUV and Hα images are prevalent and a possible source for calculating model parameters.

The most obvious model parameter to independently determine is loop length. Flare ribbons delineate the footpoints of the flare loops. Compared to 3D flare loops, ribbons are "flat" so location on the solar disk has impact on properties. To determine the location of the flare ribbon, we parameterize the ribbons using a "backbone" technique. First, a simply thresholding is done to identify the ribbon contour. Next, skeletonization is applied to thin the contour. Finally the skeleton is pruned to isolate the ribbon backbone. An example of this process is shown in Figure 12.

Figure 12: Skeletonization of flare ribbons as observed in Hα.

By applying this to a series of images, we can track the evolution of flare ribbons. Figure 13 shows this for evolution of AIA 1600 images flare ribbons.

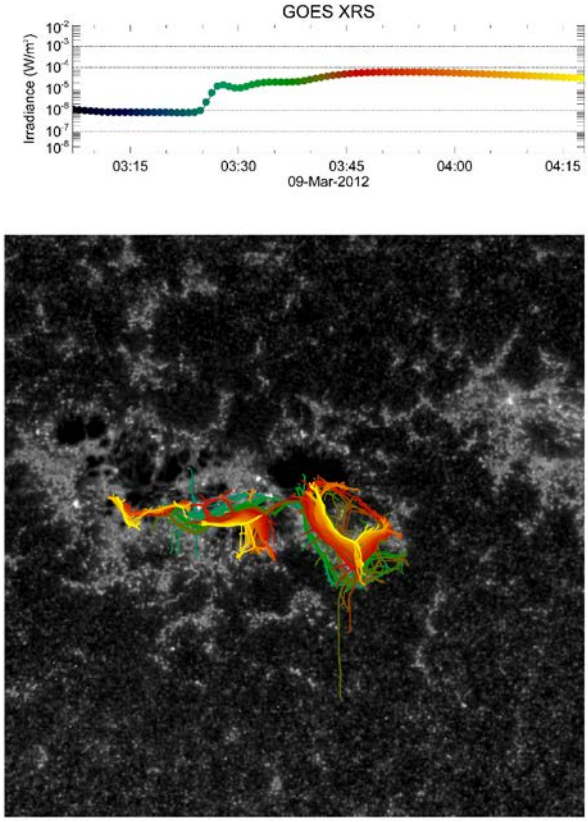

Figure 13. Temporal evolution of EUV flare ribbons at 1600 A.

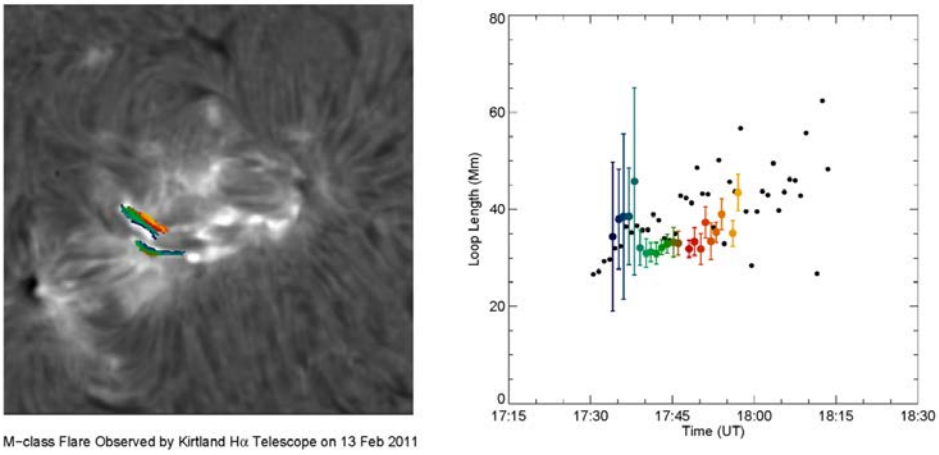

Figure 14: Temporal evolution characteristics (right) of the loop-length observed with the ISOON Ha telescope at Kirtland AFB.

Figure 14 shows for this for Hα images. Preliminary results suggest that the separation of flare ribbons can be used to estimate one of the set of AFFIM model parameters (loop length).

4. DISCUSSION AND CONCLUSIONS

The fundamental physics of solar flares, from an AF and DOD perspective is challenging in multiple ways. This research was performed from that very perspective on how to gain additional insights from a methodical perspective of forecasting solar flares. The solar atmosphere has multiple e-folding layers from (i) a basal convective dominated photosphere where the magnetic fields are pushed around by convective elements, (ii) a contested layer of the chromosphere, where the contested pressure balance between magnetic and hydrodynamic forces make it possible for the stresses in the magnetic field (related to the solar cycle) to be unleased at opportune moments when the underlying thermal conditions prevail and (iii) a hot coronal layer where the solar eruptions manifest readily, and where particle and radiative forces carry the sudden release of magnetic energy, as they are released.

At the chromospheric layer, the SCBs offer the most opportune indicators of advanced release of coronal mass ejections and large flares. They are characteristically different from the flares themselves, as evidenced in the research results presented here. SCBs can be detected at the chromospheric layer, well in advance (60 to 120 minutes) of a CME is physically observed using a space based coronagraph. In that, a regular, high cadence monitoring of solar surface chromospheres in H-alpha, offers the opportunity to develop an alert impending solar magnetic storms at its source.

The understanding of x-ray flares background variation is an important consideration for solar climatological forecasts of solar flares, advanced by months. In following the x-ray energy and its background release during the solar cycle, it is possible to develop a probabilistic forecast of the strength of an impending energy release, using the flare phase diagram.

The Air Force Flare Irradiance Model (AFFIM) is a critical tool, whose ongoing development is vital to understand the radiative effects of flares originating in the chromospheric and coronal regions of the solar atmosphere. The effects of solar flares on the terrestrial thermosphere and ionosphere, impacting orbital drag of resident space objects and on the communication disruptions due to the imposed changes on the structure of the ionosphere are vital to developing real-time forecast models that connect solar-thermosphere-ionosphere effects. These interconnected systems are an important component of the Space Environment Effects & Mitigation programs of AFRL Space Environment research.

REFERENCES

[1] Shibata, K. and Magara T., Solar Flares: Magnetohydrodynamic Processes, Living Rev. Solar Phys., Volume 8, Issue 6, http://www.livingreviews.org/lrsp-2011-6, 2011.

[2] Svestka, Z. and Cliver, E. W., History and Basic Characteristics of eruptive Flares, Eruptive Solar Flares. Proceedings of Colloquium #133 of the International Astronomical Union, (Ed.) Wilson, A., Volume SP-508 of ESA Special Publications, pp. 409-419, ESA Publications Division, Noordwijk, 2002.

[3] Aschwanden, M. J., Wuelser, J. P., Nitta, N. V., and Lemen, J. R., Solar Flare and CME Observations with STEREO/EUVI, SoPh, Volume 256, Issue 3, 2009.

[4] Lang, K. R., The Sun from Space, Springer, Berlin Heidelberg, Germany, 2009.

[5] Balasubramaniam, K. S., Pevtsov, A. A., Neidig, D. F., Cliver, E. W., Thompson, B. J., Young, C. A., Martin, S. F., and Kiplinger, A., Sequential Chromospheric Brightenings beneath a Transequatorial Halo Coronal Mass Ejection, The Astrophysical Journal, Volume 630, Issue 2, pp. 1160-1167, 2005.

[6] Balasubramaniam, K. S., Pevtsov, A. A., and Neidig, D. F., Are Moreton Waves Coronal Phenomena? The Astrophysical Journal, Volume 658, Issue 2, pp. 1372-1379, 2007.

[7] Thompson, B. J., Gurman, J. B., Neupert, W. M., Newmark, J. S., Delaboudinière, J.-P., Cyr, O. C. St., Stezelberger, S., Dere, K. P., Howard, R. A., and Michels, D. J., SOHO/EIT Observations of the 1997 April 7 Coronal Transient: Possible Evidence of Coronal Moreton Waves, The Astrophysical Journal, Volume 517, Issue 2, pp. L151-L154. 1999.

[8] Reinard, A. A. and Biesecker, D. A., Coronal Mass Ejection-Associated Coronal Dimmings, The Astrophysical Journal, Volume 674, Issue 1, article id. 576-585, 2008.

[9] Gopalswamy, N., Yashiro, S., Michalek, G., Stenborg, G., Vourlidas, A., Freeland, S., and Howard, R., The SOHO/LASCO CME Catalog, Earth, Moon, and Planets, Volume 104, Issue 1-4, pp. 295-313, 2009.

[10] Reames, D., Particle acceleration by CME-driven shock waves, AIP Conference Proceedings, Volume 516, pp. 289-300, 2000.

[11] Pevtsov, A. A., Balasubramaniam, K. S., and Hock, R. A., Sequential chromospheric brightenings: The case for chromospheric evaporation, Advances in Space Research, Volume 39, Issue 11, pp. 1781-1786, 2007.

[12] Kirk, Michael S., Balasubramaniam, K. S., Jackiewicz, Jason, McAteer, R. T. James, and Milligan, Ryan O., Properties of Sequential Chromospheric Brightenings and Associated Flare Ribbons, The Astrophysical Journal, Volume 750, Issue 2, article id. 145, 2012.

[13] Neidig, D., Wiborg, P., Confer, M., Haas, B., Dunn, R., Balasubramaniam, K. S., Gullixson, C., Craig, D., Kaufman, M., Hull, W., McGraw, R., Henry, T., Rentschler, R., Keller, C., Jones, H., Coulter, R., Gregory, S., Schimming, R., and Smaga, B., USAF Improved Solar Observing Optical Network (ISOON) and its Impact on Solar Synoptic Data Bases, in ASP Conf. Ser. 140, Synoptic Solar Physics, ed. K. S. Balasubramaniam, J. Harvey, and D. Rabin, San Francisco, CA, p. 519, 1997.

[14] Pesnell, W.D., Chamberlin, P. C., and Thompson, B. J., The Solar Dynamics Observatory, Volume 275, Issue 1-2, January 2012.

[15] Kirk, Michael S., Balasubramaniam, K. S., Jackiewicz, Jason, McAteer, R. T. James, and Milligan, Ryan O., Properties of Sequential Chromospheric Brightenings and Associated Flare Ribbons, The Astrophysical Journal, Volume 750, Issue 2, article id. 145, 2012.

[16] Kirk, M. S., Balasubramaniam, K. S., Jackiewicz, J., McAteer, R. T. J., and McNamara, B. J., Sequential Chromospheric Brightening: An Automated Approach to Extracting Physics from Ephemeral Brightening, ASP Conference Proceedings, Volume 463, Issue 267, 2012.

[17] Balasubramaniam, K. S., Pevtsov, A. A., Neidig, D. F., and Hock, R. A., Large scale solar chromospheric eruptive activity - a signature of magnetic reconnection, Proceedings of the ILWS Workshop, Goa, India, February 19-24, Editors: N. Gopalswamy and A. Bhattacharyya, ISBN: 81-87099-40-2, p. 65, 2006.

[18] Kirk, Michael S., Balasubramaniam, K. S., Jackiewicz, Jason, and McAteer, R. T. James, Qualities of Sequential Chromospheric Brightenings Observed in Halpha and UV Images, The Astrophysical Journal, Volume 796, Issue 2, article id. 78, 2014.

[19] Schrijver, C.J. and De Rosa, M.L., Photospheric and heliospheric magnetic fields, Solar Physics, Volume 212, Issue 1, pp. 165 -200, doi:10.1023/A:1022908504100, 2003.

[20] Kirk, M. S., Balasubramaniam, K.S, Jackiewicz, J., and Gilbert, H. R., The Origin of Sequential Chromospheric Brightenings, Accepted for publication in Solar Physics, 2017.

[21] Balasubramaniam, K. S. and Henry, T. W., Sunspot Numbers from ISOON: A Ten-Year Data Analysis, Solar Physics, Volume 291, Issue 9-10, pp. 3123-3138, 2016.

[**22**] Winter, L. M. and Balasubramaniam, K., Using the maximum X-ray flux ratio and X-ray background to predict solar flare class, Space Weather, Volume 13, Issue 5, pp. 286-297, 2015.

[23] Winter, L. M., Pernak, R. L., and Balasubramaniam, K. S., Comparing SSN Index to X-Ray Flare and Coronal Mass Ejection Rates from Solar Cycles 22-24, Solar Physics, Volume 291, Issue 9-10, pp. 3011-3023, 2016.

[24] Le, Huijun, Liu, Libo, and Wan, Weixing, An analysis of thermospheric density response to solar flares during 2001-2006, Journal of Geophysical Research, Volume 117, Issue A3, CiteID A03307, 2012.

[25] Helmboldt, J. F., Kassim, N. E., and Teare, S. W., Observations of the ionospheric impact of M-class solar flares on local and hemispheric scales, Earth and Space Science, Volume 2, Issue 10, pp. 387-402, 2015.

[26] Klimchuk, J. A., Patsourakos, S., and Cargill, P. J., Highly Efficient Modeling of Dynamic Coronal Loops, The Astrophysical Journal, Volume 682, Issue 2, article id. 1351-1362, 2008.

[27] Klimchuk, J. A., Patsourakos, S., and Cargill, P. J., EBTEL: Enthalpy-Based Thermal Evolution of Loops, Astrophysics Source Code Library, record ascl: 1203.007, 2012.

[28] Cargill, P. J., Bradshaw, S. J., and Klimchuk, J. A., Enthalpy-based Thermal Evolution of Loops; II. Improvements to the Model, The Astrophysical Journal, Volume 752, Issue 2, article id. 161, 2012.

[29] Cargill, P. J., Bradshaw, S. J., and Klimchuk, J. A., Enthalpy-based Thermal Evolution of Loops; III. Comparison of Zero-dimensional Models, The Astrophysical Journal, Volume 758, Issue 1, article id. 5, 2012.

DISTRIBUTION LIST

DTIC/OCP
8725 John J. Kingman Rd, Suite 0944
Ft Belvoir, VA 22060-6218 1 cy

AFRL/RVIL
Kirtland AFB, NM 87117-5776 2 cys

Official Record Copy
AFRL/RVBXT/Dr. Karatholuvu S. Balasubramaniam 1 cy